Conformations and orientations of a signal peptide interacting with phospholipid monolayers

5 AUTHORS, INCLUDING:

Richard Dluhy
University of Georgia

120 PUBLICATIONS **4,229** CITATIONS

Christopher James Mcknight
Boston University

76 PUBLICATIONS **2,428** CITATIONS

Lila M Gierasch
University of Massachusetts Amherst

234 PUBLICATIONS **11,547** CITATIONS

Conformations and Orientations of a Signal Peptide Interacting with Phospholipid Monolayers[†]

Donald G. Cornell[*]

Agriculture Research Service, Eastern Regional Research Center, U.S. Department of Agriculture, 600 East Mermaid Lane, Philadelphia, Pennsylvania 19118

Richard A. Dluhy

National Center for Biomedical Infrared Spectroscopy, Battelle—Columbus Laboratories, Columbus, Ohio 43201

Martha S. Briggs,[‡] C. James McKnight,[§] and Lila M. Gierasch[§]

Department of Chemistry, University of Delaware, Newark, Delaware 19716

Received October 24, 1988; Revised Manuscript Received December 21, 1988

ABSTRACT: The interaction of a chemically synthesized 25-residue signal peptide of LamB protein from *Escherichia coli* with phospholipids has been studied with a film balance technique. The conformation, orientation, and concentration of the peptides in lipid monolayers have been determined from polarized infrared spectroscopy, ultraviolet spectroscopy, and assay of ^{14}C-labeled peptide in transferred films. When the LamB signal peptide is injected into the subphase under a phosphatidylethanolamine–phosphatidylglycerol monolayer at low initial pressure, insertion of a portion of the peptide into the lipid film is evidenced by a rapid rise in film pressure. Spectroscopic results obtained on films transferred to quartz plates and Ge crystals show that the peptide is a mixture of α-helix and β-conformation where the long axis of the α-helix penetrates the monolayer plane and the β-structure is coplanar with the film. By contrast, when peptide is injected under lipid at high initial pressure, no pressure rise is observed, and the spectroscopic results show the presence of only β-structure which is coplanar with the monolayer. The spectroscopic and radioassay results are all consistent with the picture of a peptide anchored to the monolayer through electrostatic binding with a helical portion inserted into the lipid region of the monolayer and a β-structure portion resident in the aqueous phase. The negative charges on the lipid molecules are roughly neutralized by the positive charges of the peptide.

The roles of the signal sequence in facilitating protein export are not yet clearly defined, but its importance in this central cellular process is well established (Briggs & Gierasch, 1986). In our recent studies we have applied biophysical methods to the question of how a signal sequence may mediate the process of protein translocation across a membrane, employing signal peptides from the outer membrane protein LamB of *Escherichia coli*.[1] These synthetic signal peptides exhibit activity at the air–water interface and give evidence of interaction with lipids when injected under preformed phospholipid monolayers (Briggs et al., 1985). We have used ultraviolet, circular dichroism, and infrared spectroscopy of transferred films of peptide–lipid monolayers to characterize the conformation of the signal peptide (Briggs et al., 1986). The qualitative CD[2] and IR results led to a model for signal peptide–membrane interaction in vivo. The mechanism for peptide–membrane interaction, illustrated schematically below, involves electrostatic binding of the signal sequence to the charged lipids followed by insertion of the hydrophobic portion of the sequence into the lipid environment of the membrane. Although the conformation for each step was obtained from the CD and IR data, the orientation of the signal peptide with respect to the lipid monolayer was not known. Polarized infrared spectroscopy, used in the present work, established that the β-conformation segment of the signal peptide was coplanar with the phospholipid–water interface in all of the experiments, irrespective of whether the initial lipid pressure was low or high. At low initial film pressure, insertion of the signal peptide into the phospholipid monolayer occurred, and the polarized IR showed that the helical portion of the signal sequence spanned the monolayer. The data are consistent with a model where the helix axis is collinear with the acyl chains of the lipids. Additionally, we have quantified the peptide/lipid stoichiometry through the use of ultraviolet spectroscopy and ^{14}C-labeled peptide.

MATERIALS AND METHODS

The lipids were from Avanti Polar Lipids, Birmingham, AL. Synthesis of the full-length wild-type (WT) peptide has been described (Briggs, 1986). The radioactive peptide was syn-

[*] Address correspondence to this author.

[‡] Present address: Department of Biochemistry and Biophysics, University of Pennsylvania School of Medicine, Philadelphia, PA 19104.

[§] Present address: Department of Pharmacology, University of Texas, South Western Medical Center, 5323 Harry Hines Blvd., Dallas, TX 75235-9041.

[1] The amino acid sequence of the wild-type λ receptor protein signal sequence is

$$M_1MITL_5RKLPL_{10}AVAVA_{15}AGVMS_{20}AQAMA_{25}$$

[2] Abbreviations: CD, circular dichroism; FTIR, Fourier transform infrared; EYPE, egg yolk phosphatidylethanolamine; EYPG, egg yolk phosphatidylglycerol; POPE, palmitoyloleoylphosphatidylethanolamine; POPG, palmitoyloleoylphosphatidylglycerol; PE, phosphatidylethanolamine; PG, phosphatidylglycerol; ATR-FTIR, attenuated total reflectance–Fourier transform infrared spectroscopy; DSPC, distearoylphosphatidylcholine; CPK, Corey–Pauling–Koltun.

thesized in the same way with ^{14}C at the α-carbon of the N-terminal methionine. The spreading solvent was ACS reagent grade chloroform which had been treated with carbon black/alumina to remove traces of surface-active impurities (Cornell, 1982). The subphase was deionized, filtered water, resistivity > 10 MΩ, buffered with 5 mM Tris, pH 7.3.

A miniature Teflon trough (10 × 8 × 0.7 cm) with a dipping well (total depth 2 cm) for film transfer was used for this work. The capacity of the trough was about 100 cm³ with an air–water interface area of 80 cm². A magnetic stirrer was used to mix the peptide in the subphase. The miniature trough was mounted in the cradle of a previously described (Cornell, 1982) Langmuir balance from which the large trough had been removed. The barrier drive, Wilhelmy plate, constant pressure control, and film transfer were all provided by the large film balance system. Germanium ATR crystals (50 × 10 × 2 mm, 45°) for infrared spectroscopy were from Harrick Scientific Corp., Ossining, NY.[3]

Preparation of a peptide–lipid film for spectroscopic investigation following a set protocol: (1) cleaning of the trough and surface of the freshly poured subphase; (2) installing the Wilhelmy plate and the quartz plates (or Ge crystal); (3) spreading of the lipid film (by aliquots from chloroform solution, about 0.5 mg of lipid/mL) until the desired surface pressure was achieved (for low pressure runs) or spreading an initial amount of lipid and compressing the film if a high pressure was desired; (4) injecting the peptide (1 mg/mL in Tris, pH 7.3) into the stirred subphase and equilibrating the film (first 5 min with stirring) for 30 min; (5) transferring the film at a constant pressure to quartz plates for UV spectroscopy or a Ge crystal for IR analysis. Experiments with ^{14}C-labeled peptides followed the procedures for UV spectroscopy. Analysis of the peptide on the quartz plate was by UV spectroscopy and liquid scintillation counting according to a previous protocol (Cornell, 1984). The specific activity of the labeled peptide was determined on a stock solution whose concentration was determined by quantitative amino acid analysis.

Eight quartz plates (16 monolayers) were used for ultraviolet analysis. The single Ge crystal used for FTIR supported one monolayer on each face. The monolayers were deposited during a single pass of the substrate through the interface; multiple depositions were not attempted. The pressure–area curves for the lipid mixtures were also determined in the usual way by spreading a small amount of lipid (initial area about 250 Å²/molecule) and compressing the film in the large trough (50 × 10 × 1 cm). Spreading solutions were prepared daily from the as-received stock solution (chloroform solvent, stored at −15 to −20 °C).

FTIR spectra of the lipid–peptide monolayers were obtained after the samples were transferred to 45° germanium ATR crystals. Spectra were obtained on a Digilab FTS-10 FTIR spectrometer equipped with a narrow-band, liquid N₂ cooled HgCdTe detector at 4-cm⁻¹ resolution with triangular apodization and one level of zero filling. Spectra were obtained with a 6X ATR beam condenser accessory (Harrick Scientific) at an incoming angle of 45°. The incoming radiation was polarized with an Au wire-grid polarizer on KRS-5 (Perkin-Elmer Corp., Norwalk, CT). Typically, 4096 scans were collected to improve the signal-to-noise ratio; the spectra presented here have not been smoothed.

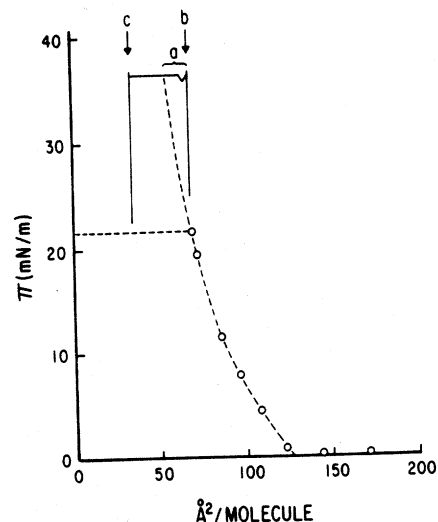Adsorption of the peptide from solution onto the quartz

FIGURE 1: Pressure–area curve of a typical peptide insertion run showing a Π–A plot (O) of a PE–PG monolayer formed by aliquot addition of lipid from chloroform solution onto 5 mM Tris, pH 7.3. After the last aliquot at about 22 mN/m, the film was equilibrated for a few minutes, and peptide (1 mg/mL in 5 mM Tris, pH 7.3) was injected into the subphase. Insertion of peptide into the monolayer caused a compression of the lipids; the average area reduction per lipid molecule (in Å²) is shown by the brace at (a). After 30 min the film was transferred to quartz plates or a Ge crystal. The plateau represents the advance in the compression barrier required to maintain constant pressure during transfer. Event markers are shown representing the (b) beginning and (c) end of the transfer. Extrapolation of the pressure–area curve (dashed line) above 22 mN/m was done with the assistance of a continuous compression curve (not shown) done on film of pure PE–PG.

plates or Ge crystal was anticipated, and contributions from this source were estimated from control experiments with monolayer films at high pressure where DSPC was the lipid. The FTIR spectra with the Ge crystal gave no evidence of peptide in the transferred films, showing that the peptide adsorbed to neither the Ge crystal nor the zwitterionic phosphatidylcholine. The UV absorption (at 190 nm) and ^{14}C count observed with quartz as the transfer substrate were thus attributed to peptide adsorption onto the silica surface. Corrections for this contribution were made for the UV and ^{14}C runs.

RESULTS

The data from a typical "low-pressure" lipid–peptide monolayer run are shown in Figure 1. For the lipid film, the pressure readings (circles) were taken 5 min after the application of each aliquot. When the desired pressure was achieved (here 22 mN/m), the peptide was injected into the subphase which caused an immediate rise in the film pressure. Most of the 15-dyn pressure rise observed occurred in the first 2–3 min of the equilibration period. The plateau between 70 and 35 Å² represents the decrease in the film area required to maintain a constant pressure (here about 37 mN/m) as the film was transferred from the air–water interface to the quartz plates. The vertical traces at 70 and 35 Å² are event markers signifying the beginning and end of the film transfer. The film transfers were efficient. The reduction in film area on the trough as transfer was effected equaled the area of the quartz plates to within about 10%. For runs where the initial lipid pressure was "high", there was no pressure rise upon injection of signal peptide into the subphase, hence no evidence of peptide insertion into the monolayer. In this case, evidence for peptide–lipid interaction came from IR and UV spectroscopy as discussed below.

---

[3] Reference to brand or firm name does not constitute endorsement by the U.S. Department of Agriculture over others of a similar nature not mentioned.
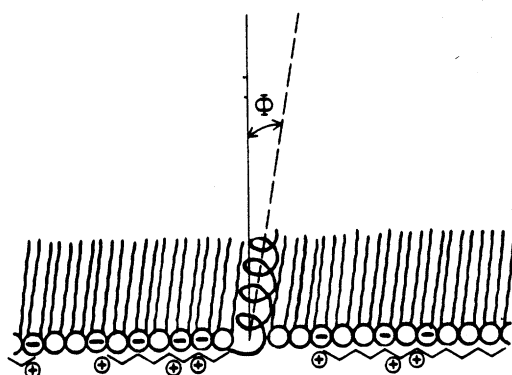
FIGURE 2: Mixed peptide–lipid monolayer showing both bound and inserted peptide. When mounted for UV or ATR-FTIR spectroscopy, the polar head group of the lipid will lie next to the mounting crystal. For UV the propagation vector of the incident light will be normal to the plane of the monolayer. For ATR-FTIR spectroscopy, the orientation of the electromagnetic radiation is given in Figure 5b.
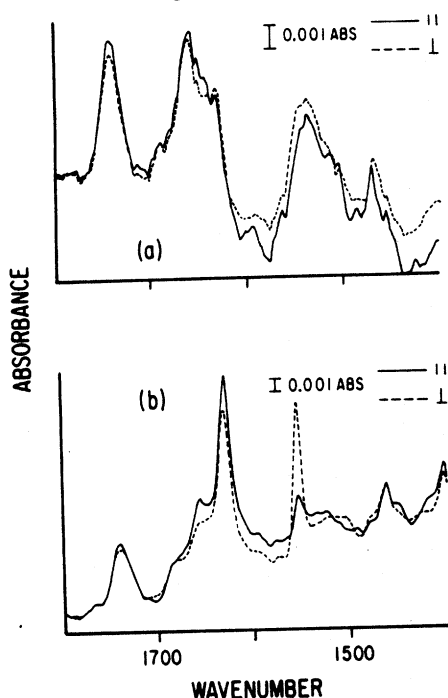

FIGURE 3: Polarized infrared spectra of the amide I and amide II bands in peptide–lipid (PE–PG) monolayers where the incident beam is polarized perpendicular ($\perp$) or parallel ($\parallel$) to the plane of incidence. The spectra are for peptide–lipid films where the initial lipid pressure was (a) low and (b) high.

Figure 2 shows, schematically, a lipid–peptide monolayer exhibiting both inserted and electrostatically bound (not inserted) peptide.

The polarized infrared (IR) spectra of the transferred monolayers are shown in Figure 3. The band near 1630 cm^{-1} in the amide I region of both the low- and high-pressure films is assignable to the β-conformation, whereas the bands at 1655–1660 cm^{-1} could be due to either the α-helix or unordered structures (Susi et al., 1967). An earlier report (Briggs et al., 1986) showed that the principle contribution to this band was from the α-helix in the low-pressure film. Since there was little evidence of helical structure in the CD of the high-pressure films (Briggs et al., 1986), the small band at 1657 cm^{-1} (Figure 6 and Table IB) probably represents only unordered structure in the bound peptide. In panels a and b of Figure 3, both the amide I and II regions are shown with the light beam polarized perpendicular ($\perp$) and parallel ($\parallel$) to the plane of incidence. The orientation of the peptide can be calculated from the observed dichroism. Table I gives the

Table I: IR Polarization Data

band		differential absorbance (mAU)	
assignment	frequency (cm^{-1})	parallel	perpendicular
(A) Low-Pressure Transfer—Signal Peptide Inserted			
lipid CH$_2$ (a)	2923.2	12.82	12.25
lipid CH$_2$ (s)	2852.4	7.81	6.67
lipid C=O	1742.3	5.87	5.35
amide I (β)	1694.7	1.71	1.48
amide I (α)	1658.3	7.38	6.65
amide I (β)	1631.1	5.49	5.15
amide II	1535.4	8.64	5.76
lipid CH$_2$	1468.9	4.70	4.68
(B) High-Pressure Transfer—Signal Peptide Bound			
lipid CH$_2$ (a)	2924.9	13.21	14.56
lipid CH$_2$ (s)	2854.9	6.24	6.51
lipid C=O	1740.8	4.97	4.20
amide I (β)	1681.2	2.45	2.26
amide I	1657.4	6.13	4.66
amide I (β)	1630.6	14.61	12.61
amide II	1554.1	3.52	11.80
lipid CH$_2$	1463.7	3.56	3.57

band intensities for the major peaks in the ATR spectra of phospholipid acyl chains and signal sequence peptides in POPE–POPG monolayers. When applied to the analysis in the Appendix, the numbers give the following results:

(A) *Conformation and Orientation of the Phospholipid Acyl Chains.* The CH$_2$ stretching bands at 2920 and 2850 cm^{-1} are conformation sensitive and have been used to determine structure and phase behavior in various phospholipid systems (Cameron & Dluhy, 1986). For insertion of signal-sequence peptides at low monolayer pressures, the measured frequency of the phospholipid CH$_2$ symmetric stretching vibration (2852 cm^{-1}) is indicative of a highly disordered hydrocarbon chain. In lipid–protein reconstituted systems, the symmetric CH$_2$ stretching vibration is preferentially used to monitor lipid acyl chain conformation, since there is a protein C–H stretching vibration at approximately 2920 cm^{-1} that overlaps with the phospholipid asymmetric CH$_2$ stretching vibration at that frequency (Mendelsohn & Mantsch, 1986). This may be the reason for the difference observed in the dichroic ratio between CH$_2$ symmetric and antisymmetric stretches for both the low and high initial pressure films (Table I). In calculating the molecular orientation of the phospholipid acyl chains in the low-pressure transferred film, we have assumed a uniaxial distribution of the hydrocarbon chain axis about the sample normal (see the discussion in the Appendix and Figure 6). The transition moments of the CH$_2$ antisymmetric and symmetric stretching modes are known to be perpendicular to the hydrocarbon chain axis (i.e., $\psi = 90°$ in Figure 6), as well as being normal to one another (Takenaka et al., 1971). Under these conditions, the orientation of the lipid acyl chains for the low surface pressure case is approximately 57° from the sample normal. This value is close to that which one would observe for a random, isotropic orientation of the lipid chains in the X–Y plane of the transferred monolayer (i.e., 54.74°). This suggests either a fluid chain tilted at an average angle of 57° from the monolayer normal or a disordered acyl chain structure. For the case of the high-pressure transferred film, the measured frequency of 2854 cm^{-1} also indicates a predominantly fluid, disordered lipid hydrocarbon in the monolayer, as in the low-pressure transfer, but with an acyl chain tilt of 20° from the membrane normal.

(B) *Conformation and Orientation of the Peptide in the Low-Pressure Monolayer.* In order to calculate the orientation of the α-helical portion of the inserted peptide, we must assume an orientation distribution for the dipole moment of the amide

Table II: Surface Concentration of Inserted Peptide and Lipid/Peptide Ratios in Low Initial Pressure Film

film	UV absorbance, 16 monolayers	no. of peptides/cm² from			charged lipid/peptide, peptides from[a]		
		film balance + CPK models	monolayer UV data	labeled peptides	CPK	UV	¹⁴C
EYPE/EYPG, 65/35 mol %	0.114	2.1 × 10¹³	2.0 × 10¹³ [2.9 × 10¹³][b]		2.4	2.5	
POPE/POPG, 65/35 mol%	0.098 (0.022)[c]	1.9 (0.1) × 10¹³	1.8 (0.4) × 10¹³ [2.5 (0.6) × 10¹³]		3.0 (0.1)	3.1 (0.8)	
POPE/POPG, 65/35 mol %, ¹⁴C-labeled peptide	0.130 (0.026)	1.5 (0.3) × 10¹³	2.3 (0.5) × 10¹³ [3.3 (0.7) × 10¹³]	2.8 (0.1) × 10¹³	3.8 (0.8)	2.5 (0.6) [1.8 (0.4)]	2.0 (0.1)

[a] The number of charged lipids (PG) varied from 5.0×10^{13} to 5.5×10^{13} molecules/cm², the total number of lipids varied from 1.4×10^{14} to 1.6×10^{14}, and the total lipid/peptide ratio varied from 5 to 11. [b] Values from isotropic or highly disordered model are shown in brackets. [c] MD of two runs shown in parentheses.

Table III: Surface Concentration of Bound Peptide and Lipid/Peptide Ratios in High Initial Pressure Films

lipid film composition	UV absorbance, 16 monolayers	no. of peptides/cm² from		no. of charged lipids/cm² (PG)[a]	charged lipid/peptide ratio
		UV data	¹⁴C-labeled peptides		
EYPE/EYPG, 65/35 mol %	0.059	8.5 × 10¹²		6.0 × 10¹³	7.1
POPE/POPG, 65/35 mol %	0.060 (0.002)[b]	8.7 (0.3) × 10¹²		7.6 (0.0) × 10¹³	8.7 (0.3)
POPE/POPG, 65/35 mol %, ¹⁴C–labeled peptide	0.104 (0.002)	1.5 (0.0) × 10¹³	2.4 (0.3) × 10¹³	6.5 (0.1) × 10¹³	[4.3 (0.1)][c] [2.7 (0.3)][d]

[a] The total number of lipids varied from 1.7×10^{14} to 2.2×10^{14}, and the total lipid/protein ratio varied from 8 to 25. [b] MD of two runs shown in parentheses. [c] From UV data. [d] ¹⁴C data.

I vibration with respect to the α-helix axis (ψ in Figure 6). Literature values for ψ range from 22.6° (Nabedryk et al., 1982) to 39° (Tsuboi, 1962). From the model described in detail in the Appendix, these values produce a range of expected values for the orientation of the peptide α-helix axis of between 58° and 61° from the membrane normal. This range of values coincides very well with the value of 57° calculated for the orientation of the phospholipid acyl chains in the low-pressure insertion experiment. These calculations suggest a model where the signal-sequence peptide inserts into the phospholipid monolayer with the helix axis collinear with the phospholipid acyl chains in a film where both the peptide helix and lipid acyl chains exhibit considerable randomness around the average distribution.

(C) *Conformation and Orientation of the Peptide in the High-Pressure Monolayer.* The infrared frequencies for the amide I vibration (Figure 3 and Table I) for the high-pressure transfer clearly indicate that the peptide's conformation is predominantly β-structure. The polarized spectra of the high-pressure film show that the amide II vibration is polarized in the perpendicular (*Y*) orientation, indicating that the β-structure is oriented primarily along the surface of the crystal, in the plane of the membrane monolayer.

Estimates of the number of lipids and peptides and the resulting lipid/peptide ratios from the monolayer runs are given in Table II for the low-pressure runs and in Table III for the high-pressure runs. The number of lipid molecules per square centimeter for both the low- and high-pressure runs is readily calculated from the film preparation conditions. The number of peptide molecules in the monolayers was estimated from ultraviolet spectra of the transferred films and, in the case of the low-pressure films where penetration occurs, geometric arguments involving molecular models as outlined below. For one run (in duplicate) radioassay of ¹⁴C-labeled peptide gave accurate results for the number of peptides per unit area of monolayer, in addition to the estimates from the UV and geometric approaches.

To calculate the peptide concentration in the monolayer films from surface area and UV spectroscopic data, we must be able to estimate the surface area of the interacting species and determine the effect of molecular orientation on the ul-

traviolet spectra of the system. For geometric estimates of the peptide surface area in the low-pressure runs, we assumed that the peptide inserted through the monolayer, normal to the plane of the interface, and that sufficient compression of the lipid molecules occurred to give the observed pressure rise. The compression required was estimated from a separate pressure–area curve of a film containing only lipid (not shown). The area reduction for the lipid fraction arrived at in this way varied between 17 and 21% for the work reported here. It was assumed that in the mixed film, the lipid occupied the reduced area with peptide in the remaining space. The number of peptide molecules that could fit into this space was calculated[4] by assuming 100 Å² for the cross-sectional area of the wild-type peptide in an α-helical conformation.[5] This of course gives us an estimate for only the perfectly oriented case, but it serves as a useful comparison with the values obtained from the UV and ¹⁴C data. To calculate the number of peptide molecules from the ultraviolet data, the molar absorptivity of the peptide must be known. Since this parameter is conformation and orientation dependent, attempts to determine it experimetally on an isotropic solution of peptide in an unspecified conformation will not suffice. We have used a calculated estimate based on the assumed model (Figure 2) and literature data on backbone and side-group contributions and the known effects of orientation. The spectra of the side groups that contribute significantly to the UV absorption at 190 nm have been given (McDiarmid, 1965). Their sum (4 Met + Gln + Arg) is 25 700 L mol⁻¹ cm⁻¹. The molar (residue) absorptivity of proline at 190 mm is about the same (5200 L mol⁻¹ cm⁻¹) in both polyprolines I and II (Fasman & Blout, 1963; Gratzer et al., 1963). For the backbone contribution to the absorption spectra we used a residue absorptivity of 4300 L mol⁻¹ cm⁻¹ (α-helix) and 6400 L mol⁻¹

_____

[4] Implicit in this procedure is the assumption that the areas of the peptide and lipid in the mixed film are strictly additive where the total area of the mixed film can be calculated from specific areas obtained from pressure–area curves of the pure components. Film balance experiments with fragments of wild-type peptide and PE–PG lipids have shown that additivity is observed (James D. Lear, private communication).

[5] L. M. Gierasch, unpublished observation.

cm⁻¹ (β-sheet) (Rosenheck & Doty, 1961).

We based our calculations on two conformational models for the interaction of peptide with lipid monolayers. In the instance where the peptide interacts with a lipid monolayer at low initial pressure, there is spectroscopic evidence for both α-helix and β-conformation. We chose a model with 16 residues (10–25) in an α-helix, Pro at 9, and 8 residues (1–8) of β-conformation. In the case where peptide interacts with a lipid monolayer at high initial pressure, only the β-conformation is observed, and we have simply β-structure at 1–8 and 10–25 plus Pro at 9.

In addition to calculating the contribution of each side-group and backbone portion to the overall UV absorption of the peptide, account must be taken of the fact that we are dealing with species oriented in films rather than rapidly tumbling molecules in isotropic solution. In spectroscopic measurements the absorbance is proportional to $\cos^2 \theta$ where θ is the angle between the absorption transition moment of the molecule and the electric vector of the impinging light. In isotropic solution $\cos^2 \theta$ is 1/3; in an idealized film for the case where the transition moment and the electric vectors are coplanar, $\cos^2 \theta$ is 1/2 (Gratzer et al., 1961). In the monolayer films studied here, the propagation vector of the incident light is normal to the monolayer plane and the electric vector lies in the plane of the film. The 190-nm transition moment of the α-helix is perpendicular to the helix axis (Gratzer et al., 1961); in the β-sheet the 190-nm moment is in plane (Pysh, 1966). Thus for the peptide–lipid monolayer shown in Figure 2, all of the transition moments of the peptide backbone in the 190-nm band, both β-structure and α-helix, are coplanar with the electric vector of the ultraviolet light. In this case, an enhancement of 50% in absorption intensity of the 190-nm bands in the films as compared to isotropic solution is to be expected (Gratzer et al., 1961). The side-chain and proline contributions to the 190-nm band were treated as isotropic additions to the UV absorption in the absence of structural information for these groups.

The adjustments to the molar absorptivity of the peptides to account for the effects of orientation amounted to about a 40% enhancement over the isotropic case for both models. This means of course that a correspondingly fewer number of peptides will be required to give the observed UV absorption in the oriented films than in an isotropic sample. We then calculated the number of peptides in the monolayer from the ultraviolet absorbance using what is essentially Beer's law for films, namely

$$A = n\epsilon\Gamma/6.02 \times 10^{20} \qquad (1)$$

where A is the absorbance of n monolayers, ϵ is the molar absorptivity of the peptide, and Γ is the number of peptides per square centimeter in a single monolayer. The factor $n\Gamma/6.02 \times 10^{20}$ has the same dimensionality (mass per squared length) and numerical value as the lc product (path length in centimeters times concentration in moles per liter) of the classical Beer's law for solutions.

Radioassay gave an accurate analysis for the number of ¹⁴C-labeled peptides per unit area of transferred film that required no assumptions about the conformation or orientation of the peptide in the monolayer. The accuracy of the analysis was assured by counting each sample until the error (2σ) was 2% or less. The results of the radioassay supports the UV data in Tables I and II and show that agreement is best for the case where, in the UV analysis, the peptide orientation was assumed to be isotropic. Taken together, the ¹⁴C and spectroscopic results show that while the UV method can give an estimate of the number of peptides in monolayer films, it can be es-

pecially useful when used in conjunction with an independent method for peptide assay.

DISCUSSION

The picture of peptide interaction with lipid monolayers that has evolved during the course of this work involves two steps; first the electrostatic binding of a positively charged peptide to the negatively charged lipid film followed by insertion of a portion of the sequence into the hydrophobic region of the monolayer. A mechanism for the initial steps in protein export which incorporate these features has been proposed (Briggs et al., 1986). The involvement of the signal sequence in the mechanism may be summarized as (1) the approach of a random peptide to the membrane surface, (2) electrostatic binding of the peptide to the membrane surface, possibly in the β-conformation, and followed by (3) insertion of the hydrophobic portion of the sequence into the lipid environment of the bilayer. At some point in the process, a portion of the peptide assumes the α-helical conformation. In this paper, we have formulated a quantitative picture of peptide–monolayer interactions which suggests some very plausible refinements of the protein translocation model.

In previous work with signal peptide in sonicated PE–PG vesicles, CD spectra were obtained that corresponded to 60% α-helix, on the basis of mathematical fitting to reference spectra (Briggs, 1986; Greenfield & Fasman, 1969). Inspection of the sequence for the LamB wild-type peptide shows that the segment from 10 to 25 is favorable for a α-helical formation, especially in a lipid environment, and thus, it is likely to reside in the hydrocarbon portion of the phospholipid monolayer. The positive charges at 1, 6, and 7 suggest that this portion of the peptide is involved in electrostatic binding to the negatively charged PG molecules and remains in the aqueous phase. Anchoring of this segment of the molecule to a planar monolayer would seem to favor a β-conformation. All of this suggests a model with about 60% α-helix (10–25) and 30% β-sheet if we assume the β-configuration for the 1–8 residues. This is consistent with both the CD and IR spectra which show a mixture of α-helix and β-conformation for the peptides in the low-pressure runs. An alternate explanation of a mixture of pure α and pure "other" peptides seems less reasonable because of the helix breaking Pro at 9 in the wild-type sequence.

In the early phase of this work, estimates of the number of peptides inserted into the low-pressure film obtained from ultraviolet spectroscopy and film balance measurements were in good agreement when the model was one of a highly ordered system where the helical portion of the peptide spanned the lipid film with its helix axis normal to the plane of the monolayer. The results of polarized infrared measurements, however, showed considerable disorder in both the acyl chains of the lipids and the helical portion of the peptides. To resolve this apparent discrepancy, ¹⁴C-labeled wild-type peptides and radioassay were used to give an accurate determination of the peptide concentration in the transferred films that was independent of any conformation or orientation model. As can be seen from Table II, the ¹⁴C results for the number of peptides in the monolayer lie between the spectroscopic estimates for the perfectly ordered and completely disordered cases. The data in Table II are thus consistent with a picture of the peptide spanning the lipid monolayer where both the lipid and peptide exhibit considerable disorder. The charged lipid/peptide ratio (2–3) suggests a rough balance between the negatively charged lipids (one charge per molecule) and the positively charged peptide (three charges per molecule). The charged lipid/peptide ratio of about 2 obtained with the

[14]C-labeled peptide and the disordered peptide–UV data suggests that the adjacent charges at 6 (Arg) and 7 (Lys) may be too close to each other to be involved in electrostatic binding with more than one lipid. The estimates for the number of peptides inserted into the monolayer tended to be lower when film balance data and CPK models were used than when UV and ^{14}C data were employed. This suggests that the assumption of additivity for the full-length wild-type peptide may not be true. More peptides may be able to pack into the available space in the lipid film than strict additivity would allow, resulting in a condensed film. Negative deviation from ideality frequently occurs between interacting species (Cadenhead et al., 1980). Alternately, some bound peptide may reside entirely in the aqueous phase and not contribute to the pressure rise observed in the low initial pressure films.

Insertion of the peptide through the monolayer where the helix axis is collinear with the acyl chains of the lipids is certainly plausible for a molecule where the hydrophobic α-helix and the charged groups are localized at opposite ends of the structure. Recently, incorporation of a synthetic mitochondrial signal peptide into lipid monolayers has been reported where the evidence was consistent with an α-helix with its long axis parallel to the plane of the interface (Tamm, 1986). In that case, however, the peptide studied exhibited a side-to-side amphiphilicity rather than the end-to-end amphiphilicity of the LamB peptide, and an orientation with the helix axis in the monolayer plane would be favored.

Two reports on the interfacial behavior and structure of the signal sequence of *E. coli* outer membrane pore protein PhoE and its interaction with phospholipid model membranes have recently appeared (Batenburg et al., 1988a,b). The investigations involved film balance techniques and computer modeling of the interfacial area occupied by peptides in various conformations and orientations. Their results suggested that the PhoE signal sequence, which exhibits end to end amphiphilicity, spanned a phospholipid monolayer. This is consistent with our findings presented here. Taken together, the results of all of these reports suggest the importance of the hydrophobic and hydrophilic makeup of signal sequences in determining how they interact with a lipid environment.

In the high-pressure films where insertion does not occur, the peptide bound to the monolayer is almost entirely in the β-conformation. The estimates (from the ultraviolet data) for the number of peptides bound per square centimeter of lipid film varied between 0.9×10^{13} and 1.5×10^{13}, suggesting an average area per peptide of about 700–1200 Å^2. The number of bound peptides from the ^{14}C data, 2.4×10^{13} peptides/cm^2, suggests an average coverage per peptide of about 420 Å^2. The UV calculations are based on a model of a perfectly ordered species. Any disorder in the film would result in a lower UV molar absorptivity with a corresponding increase in the estimate of the number of peptides per square centimeter in the monolayer. A reasonable estimate for the area occupied by a contiguous film of peptides in the β-conformation is about 20 Å^2/residue (DeGrado & Lear, 1985) which gives an area of 500 Å^2/molecule for the wild-type peptide in a tightly packed β-sheet. From this we conclude that the peptide is probably bound to the lipid monolayer in a contiguous, somewhat disordered film. Although the polarized infrared spectrum suggests a net orientation of the peptide β-sheet that is coplanar with the lipid monolayer, a quantitative measure of the degree of orientation cannot be made with the available IR data.

All of the spectroscopic information in this work was obtained on films transferred from the air–water interface to a
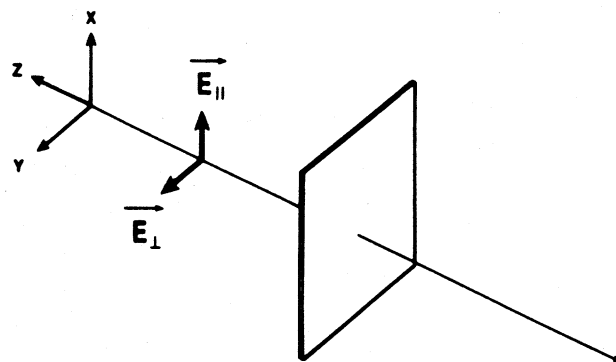

FIGURE 4: Schematic of the incident electric fields in polarized transmission spectroscopy. $E_{\parallel}$ is the parallel orientation and $E_{\perp}$ is the perpendicular orientation with respect to the plane of incidence (XZ).

solid substrate, either germanium or quartz. The applicability of experimental results obtained with films on solid substrates to films on the surface of water depends in part on the preservation of the structure of the monolayer during transfer. In the current work the reduction in film area on the trough during constant-pressure transfer equaled the area of the quartz plates (to within 10%, vide supra), suggesting that transfer was "quantitative" for this substrate. For the conclusions drawn from the IR spectra, the fact that a difference was observed in orientation of the phospholipid acyl chains between low and high initial pressure films suggests that this was a feature of the monolayers at the air–water interface and was preserved during transfer to the germanium crystals. Nevertheless, although gross structural features appear to have been preserved during transfer to both quartz and Ge, viscous drag induced in the films by the transfer process and the anchoring of the film to a solid substrate could well cause some perturbation of the molecular structure. This possibility should be kept in mind when the findings presented here are being considered.

Our results clearly suggest that the peptide binds to the monolayer and assumes the β-conformation at the lipid–water interface in the case where the initial film pressure is high and insertion is prevented. In the case where the initial pressure is low, insertion occurs and the film pressure rises markedly. What is uncertain in this case is whether at equilibrium any of the bound peptide remains entirely in the aqueous phase in the β-conformation. Since the spectroscopic evidence shows β-structure as well as α-helix in the cases where peptide insertion occurs, that possibility cannot be excluded although it does not have to be postulated to explain any of our findings with the low initial pressure films.

We have studied several synthetic signal peptides in dilute aqueous solution, complexed with sodium dodecyl sulfate (SDS), and in vesicle suspensions (Briggs, 1986) (McKnight, Briggs, and Gierasch, unpublished results). The wild-type peptide can form any of the three principal conformations, α-helix, β-sheet, or unordered, depending on the environment. For full-length WT peptides, dilute aqueous solution favored the unordered conformation, while complexation with SDS or vesicle suspensions favored α-helix with formation of some β-sheet and unordered structure. The current work shows that, in the presence of a strong organizing influence such as a lipid monolayer, very little unordered structure is observed but, depending on the particular film conditions, either of the ordered conformations, α-helix or β-structure, may be favored.

The present results thus reinforce the picture of a signal peptide spontaneously inserting into a lipid monolayer and spanning the hydrophobic portion of the film. As suggested
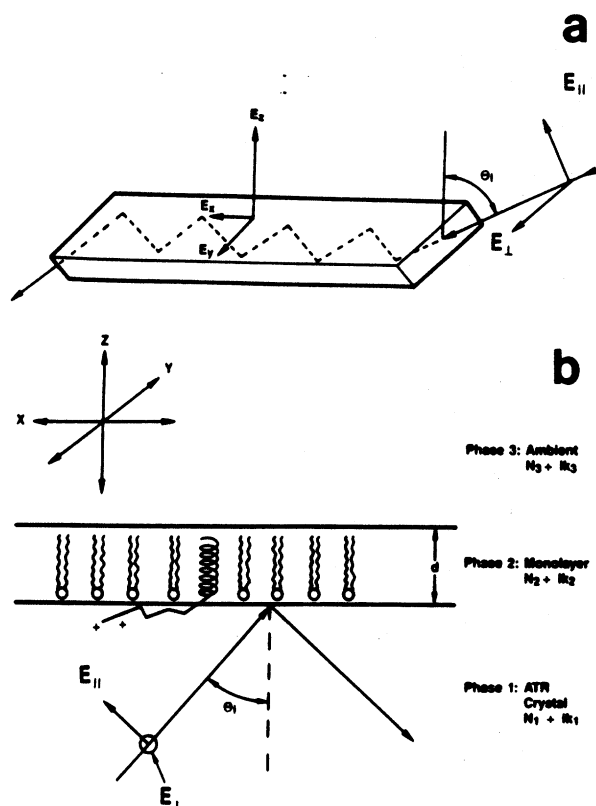
FIGURE 5: Schematic illustration of the interaction of plane-polarized electromagnetic radiation with the infrared attenuated total reflectance (ATR) crystals used in the current experiments. (a) Parallel (∥) and perpendicular (⊥) components are shown for the incoming propagating wave as well as the resulting electric field (E_x, E_y, and E_z). θ_1 is the incoming angle of incidence. (b) Diagram illustrating the interaction of a plane electromagnetic wave in a three-phase (crystal–monolayer–ambient) system.
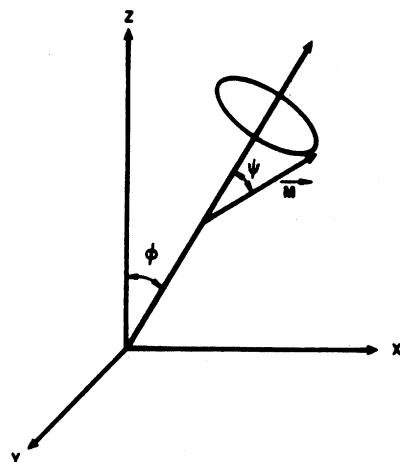

FIGURE 6: Schematic illustration of the relationship between the measured ATR dichroic ratio and the assumed uniaxial orientation of the peptide bonds. In this scheme, the X, Y, and Z directions refer to the coordinate geometry of the ATR crystal (see Figure 5), ψ is the angle between the peptide axis and the bond dipole moment M, and ϕ is the average orientation angle between the peptide axis and the surface normal (i.e., Z direction).

earlier (Briggs et al., 1986), this behavior likely reflects a major role of the signal sequence in protein translocation.

ACKNOWLEDGMENTS

APPENDIX

(A) *Ultraviolet Spectroscopy*. There are two models to be considered for the interaction of wild-type peptide with phospholipid monolayers: (1) Low initial lipid pressure where the peptide inserts into the monolayer. Here there is spectroscopic evidence for both the α-helix and the β-conformation. (2) High initial lipid pressure where the peptide does not appear to be inserted but only electrostatically bound to the lipid. In this case the spectroscopic evidence suggests that the peptide is principally in the β-conformation.

We used information from the literature on backbone (Rosenheck & Doty, 1961), side-group (McDiarmid, 1965), and proline (Fasman & Blout, 1963; Gratzger et al., 1963) contribution to the molar absorptivity of peptides at 190 nm and the known effects of orientation (Gratzer et al., 1961). Applying this information to the models discussed above leads to the following estimates of the molar absorptivity of the oriented peptides:

(a) Low-pressure run. Sixteen residues in perpendicular α-helix, eight residues in parallel β-conformation, one proline, and six side groups:

$$\epsilon = (1.5)(16)(4300) + (1.5)(8)(6400) + 5200 + 25\,700 = 210\,900 \text{ L mol}^{-1} \text{ cm}^{-1} \quad (A1)$$

Mean residue absorptivity is about 8400 L mol^{-1} cm^{-1} for the oriented polymer and about 6000 L mol^{-1} cm^{-1} for the isotropic case.

(b) High-pressure run. Twenty-four residues in parallel β-conformation, one proline, and six side groups:

$$\epsilon = (1.5)(24)(6400) + 5200 + 25\,700 = 261\,300 \text{ L mol}^{-1} \text{ cm}^{-1} \quad (A2)$$

Mean residue absorptivity for the oriented polymer is about 10 500 L mol^{-1} cm^{-1}; for the isotropic case, it is 7400 L mol^{-1} cm^{-1}.

(B) *Calculation of Molecular Orientation for Thin Films Using Polarized ATR–Infrared Spectroscopy*. The calculation of the molecular orientation for monolayers and thin films adsorbed onto ATR crystals is more complicated than the case when polarized transmission at normal incidence is used. Essentially, the differences arise because for transmission spectroscopy the incident electric fields are conveniently regarded as equal to 1. That is, there is no difference in the intensity between the parallel-polarized and perpendicular-polarized radiation (Figure 4). This is not the case for the electric fields at the surface of an ATR crystal. The geometry of the ATR crystal (Figure 5a) requires that there be three components of the electric field present at the crystal surface. The magnitude of these three electric field vectors depends upon the angle of incidence of the radiation on the crystal and the optical constants of the three phases (crystal, thin film, and ambient). For example, for a germanium crystal with a 45° angle of incidence, the mean square electric field intensities present at the air–germanium interface (assuming the incident fields are equal to 1) are $\langle E_x^2 \rangle = 1.991$, $\langle E_y^2 \rangle = 2.133$, and $\langle E_z^2 \rangle = 0.009$. Among other things, the disparity between these values must be taken into account when orientation effects for anisotropic samples are calculated.

The procedure for calculating orientation of thin film samples involves two distinct steps. These are (1) calculation of the unique optical parameters (e.g., electric field intensities and absorption equation variables) that are inherent in the ATR experiment and that are necessary to take into account in the final determination of a corrected ATR dichroic ratio, R_{ATR}, and (2) use of this corrected dichroic ratio (R_{ATR}) in a defined model for molecular orientation (e.g., uniaxial, bi-

axial, etc.) to calculate orientation distributions.

(a) Calculation of Optical Effects. The interaction of plane-polarized radiation with monolayers and/or thin films that have been transferred onto a solid support is mathematically treated in terms of the optical physics of a three-phase stratified-layer system (i.e., crystal, thin film, and ambient, Figure 5b). These equations have been derived in several forms [see, for example, Born and Wolf (1970), Heavens (1965), Hansen (1968), or McIntyre (1973)]. The essential input parameters to these equations are the angle of incidence of the radiation on the surface (θ) and the optical constants (n and k) of the three phases. Several values are possible for the optical constants for the first (i.e., ATR crystal) phase, depending on the choice of crystal. In our case, for germanium, $n_1 = 4.0$ and $k_1 = 0.0$. The optical constants for the thin film are, in general, unknown. We can, however, make the reasonable approximation that $n_f = 1.5$ for the thin film phase; for k_f, a value of 0.1 is reasonable for even strongly absorbing IR bands. The ambient (third) phase is usually air; hence, $n_3 = 1.0$ and $k_3 = 0.0$.

For monolayers and very thin films (i.e., those films where $d < 0.01\lambda$, where d is the film thickness and λ is the wavelength), the electric fields present in the film may be assumed to be identical with the film-free two-phase system (i.e., crystal and ambient) (Hansen, 1972, 1973). We therefore calculate the mean square electric fields ($\langle E^2 \rangle$) at the air–germanium boundary by the use of the following equations (Hansen, 1968, 1972, 1973):

$$\langle E_\perp{}^2 \rangle = (1 + R_\perp) + 2R_\perp{}^{1/2} \cos[\delta^r_\perp - 4\Pi(z/\lambda)\xi_1]$$

$$\langle E_{\parallel x}{}^2 \rangle = (\cos^2 \theta)[(1 + R_\parallel) - 2R_\parallel{}^{1/2} \cos[\delta^r_\perp - 4\Pi(z/\lambda)\xi_1]]$$

$$\langle E_{\parallel z}{}^2 \rangle = (\sin^2 \theta)[(1 + R_\parallel) + 2R_\parallel{}^{1/2} \cos[\delta^r_\parallel - 4\Pi(z/\lambda)\xi_1]]$$

where $R_\parallel$ is the overall reflectance for parallel polarization, $R_\perp$ is the overall reflectance for perpendicular polarization, and z is the distance from the phase boundary.

In these equations, θ is the angle of incidence of the incoming infrared radiation (relative to the normal to the interface), and ξ_1 is angle-dependent refractive index term equal to

$$\xi_1 = (\hat{n}_1 - n_1{}^2 \sin^2 \theta)^{1/2}$$

where n is the complex refractive index term ($\hat{n} = n + ik$) and δ^r_i is defined as the phase change on reflection for polarization i ($i = \parallel$ or $\perp$) and is defined by

$$\delta^r_i = \tan^{-1}(\mathrm{Im}\, r_i / \mathrm{Re}\, r_i)$$

In this case, r_i is the Fresnel reflection coefficient for polarization i and z is the distance from the first phase boundary. After calculation of the expected electric fields, the next task is to relate these fields to the reflection–absorption of each polarization. Hansen (1972, 1973) has derived general approximate equations for the changes in reflectivity caused by the presence of a thin film in attenuated total reflectance. For perpendicular polarization

$$\Delta A_\perp = \frac{n_f \alpha_y dN}{2.3 n_1 \cos \theta} \langle E_\perp{}^2 \rangle \tag{B1}$$

and for parallel polarization

$$\Delta A_\parallel = \frac{n_f \alpha_x dN}{2.3 n_1 \cos \theta} \langle E_{\parallel x}{}^2 \rangle + \frac{n_f \alpha_z dN}{2.3 n_1 \cos \theta} \frac{n_1{}^4}{(n_f{}^2 + k_f{}^2)^2} \langle E_{\parallel z}{}^2 \rangle \tag{B2}$$

In eq B1 and B2 ΔA_i is the peak height measured relative to

the base line for polarization i (where $i = \parallel$ or $\perp$), n_1 is the refractive index of the crystal, n_f is the refractive index of the film, d is the film thickness, N is the total number of reflections on the ATR crystal, and k_f is the extinction coefficient of the film. In general, the extinction coefficient is anisotropic and has separate components along the x, y, and z axes (i.e., k_x, k_y, and k_z). The parameter α_j is the Lambert absorption coefficient of the film in the jth orientation (where $j = x, y,$ or z) and is related to k_j by

$$\alpha_j = \frac{4\pi k_j}{\lambda} \tag{B3}$$

The fact that the sample extinction coefficient (k_f) is anisotropic ensures that the overall absorption coefficient α_f will also be geometry dependent, as the above equation states.

The electric fields are calculated at the air–crystal boundary in the first phase by use of eq B1–B3. Note that the equation for parallel polarization has two terms due to the components (x and z) of parallel polarized radiation.

Experimental conditions specify that $n_1 = 4.0$, $n_3 = 1.0$, and $\theta = 45°$. We have assumed approximate values for n_f and k_f and can thus calculate the electric fields. We also measure $\Delta A_\perp$ and $\Delta A_\parallel$ from the spectra, which reduces eq B1 and B2 to

$$\Delta A_\perp = A\alpha_y d \tag{B4}$$

$$\Delta A_\parallel = B\alpha_x d + C\alpha_z d \tag{B5}$$

where A, B, and C are constants.

We then wish to calculate $\alpha_x d$, $\alpha_y d$, and $\alpha_z d$, since these will give us k_x, k_y, and k_z and allow us to unambiguously determine molecular orientation. In practice this is not possible for two reasons: (1) we do not explicitly know d (film thickness), and (2) eq B4 and B5 are inherently underdetermined since we wish to calculate three unknowns in two equations. However, in certain cases we can make the assumption that the transferred monolayer has a uniaxial distribution about the surface normal (vide infra). This implies that the anisotropic absorption coefficients for the in-plane surface components of the film (i.e., $\alpha_x d$ and $\alpha_y d$) are equal. If this relationship (i.e., $\alpha_x d = \alpha_y d$) is now combined with eq B4 and B5, we can calculate values for the anisotropic absorption coefficients $\alpha_x d$, $\alpha_y d$, and $\alpha_z d$. This assumption also allows us to calculate a corrected dichroic ratio for the monolayer/thin film in the ATR experiment, namely

$$R_{ATR} = \frac{\Delta A_\parallel}{\Delta A_\perp} = \frac{B}{A} + \frac{C}{A}\frac{\alpha_z}{\alpha_x} \tag{B6}$$

Similar analyses have been presented for ATR-FTIR spectra of other transferred monolayers and thin films (Higashiyama & Takenaka, 1974; Takenaka et al., 1980; Okamura et al., 1985).

(b) Orientation Model. Once the corrected dichroic ratio for the ATR experiment has been calculated, the problem reduces to quantitatively correlating the calculated dichroic ratio with the actual structure and orientation of the molecule. This can be done only indirectly in the absence of the anisotropic extinction coefficients of the sample (i.e., k_x, k_y, k_z). In this case we assume a model for the molecular orientation and apply the corrected dichroic ratio (R_{ATR}) to calculate the orientation distribution.

A reasonable orientation to assume for transferred monolayers of chain molecules is uniaxial orientation. In this type the orientation is isotropic in the plane perpendicular to the sample normal with the sample aligned along a defined angular distribution ϕ from the normal axis. This type of orientation

has been theoretically treated (Zbinden, 1964; Fraser & MacRae, 1973) and is shown in Figure 6.

It can be shown that an oriented polymer with chain symmetry can be described by an orientation distribution function $P(\phi)$ where ϕ is the angle between the chain and the Z axis. This orientation distribution function is given by the spherical harmonic (Rothschild & Clark, 1979; Jasse & Koenig, 1979):

$$P(\theta) = \sum_{n=0}^{\infty} (N + 1/2)[\overline{P_n(\cos \phi)}]P_n(\cos \phi)$$

It can be shown that the observed infrared dichroic ratio is related to this orientation distribution function by (Jasse & Koenig, 1979)

$$\overline{P_2(\cos \phi)} = \frac{1}{2}[3(\overline{\cos^2 \phi}) - 1] = \frac{(R-1)(R_0 + 2)}{(R - 2)(R_0 - 1)} \qquad \text{(B7)}$$

where $R_0 = 2 \cot^2 \psi$ and ψ = the angular distribution of the transition dipole moment with respect to the chain axis. In our case, we use R_{ATR}, the corrected infrared dichroic ratio calculated in eq B6, as the observed infrared dichroic ratio (R) in eq B7 to calculate the orientation distribution function.

REFERENCES

Batenburg, A. M., Brasseru, R., Ruysschaert, J.-M., Van Scharrenburg, G. J. M., Slotboom, A. J., Demel, R. A., & De Kruijff, B. (1988a) *J. Biol. Chem. 263*, 4202–4207.

Batenburg, A. M., Demel, R. A., Verkleij, A. J., & De Kruijff, B. (1988b) *Biochemistry 27*, 5687–5685.

Born, M., & Wolf, E. (1970) *Principles of Optics*, Pergamon Press, New York.

Briggs, M. S. (1986) Ph.D. Dissertation, Yale University, New Haven, CT.

Briggs, M. S., & Gierasch, L. M. (1986) *Adv. Protein Chem. 38*, 109–180.

Briggs, M. S., Gierasch, L. M., Zlotnick, A., Lear, J. D., & DeGrado, W. F. (1985) *Science 228*, 1096–1099.

Briggs, M. S., Cornell, D. G., Dluhy, R. A., & Gierasch, L. M. (1986) *Science 233*, 206–208.

Cadenhead, D. A., Müller-Landau, F., & Kellner, B. M. J. (1980) in *Ordering in Two Dimensions* (Sinha, S. K., Ed.) p 73, Elsevier/North-Holland, New York.

Cameron, D. G., & Dluhy, R. A. (1986) in *Spectroscopy in the Biomedical Sciences* (Gendreau, R. M., Ed.) p 53, CRC Press, Boca Raton, FL.

Cornell, D. G. (1979) *J. Colloid Interface Sci. 70*, 167–180.

Cornell, D. G. (1982) *J. Colloid Interface Sci. 88*, 536–545.

Cornell, D. G. (1984) *J. Colloid Interface Sci. 98*, 283–285.

DeGrado, W. F., & Lear, J. D. (1985) *J. Am. Chem. Soc. 107*, 7684–7689.

Fasman, G. D., & Blout, E. R. (1963) *Biopolymers 1*, 3–14.

Fraser, R. D. B., & MacRae, T. P. (1973) *Conformation in Fibrous Proteins and Related Synthetic Peptides*, Academic Press, New York.

Gratzer, W. B., Holzwarth, G. M., & Doty, P. (1961) *Proc. Natl. Acad. Sci. U.S.A. 47*, 1785–1791.

Gratzer, W. B., Rhodes, W., & Fasman, G. D. (1963) *Biopolymers 1*, 319–330.

Greenfield, N., & Fasman, G. D. (1969) *Biochemistry 13*, 4108–4115.

Hansen, W. N. (1968) *J. Opt. Sci. Am. 58*, 380–390.

Hansen, W. N. (1972) *Prog. Nucl. Energy, Ser. 9 11*, 3–35.

Hansen, W. N. (1973) *Adv. Electrochem. Electrochem. Eng. 9*, 1–60.

Heavens, O. S. (1965) *Optical Properties of Thin Solid Film*, Dover, New York.

Higashiyama, T., & Takanaka, T. (1974) *J. Phys. Chem. 78*, 941–947.

Jasse, B., & Koenig, J. L. (1979) *J. Macromol. Sci., Rev. Macromol. Chem. C17(1)*, 61–135.

McDiarmid, R. S. (1965) Ph.D. Thesis, Harvard University, Cambridge, MA.

McIntyre, J. D. E. (1973) *Adv. Electrochem. Electrochem. Eng. 9*, 61–166.

Mendelsohn, R., & Mantsch, H. H. (1986) *Prog. Protein–Lipid Interact. 2*, 103.

Nabredryk, E., Gingold, M. P., & Breton, J. (1982) *Biophys. J. 38*, 243–249.

Okamura, E., Umemura, J., & Takenaka, T. (1985) *Biochim. Biophys. Acta 812*, 139–146.

Pysh, E. S. (1966) *Proc. Natl. Acad. Sci. U.S.A. 56*, 825–832.

Rosenheck, K., & Doty, P. (1961) *Proc. Natl. Acad. Sci. U.S.A. 47*, 1775–1785.

Rothschild, K. J., & Clark, N. A. (1979) *Biophys. J. 25*, 473–488.

Susi, H., Timasheff, S. N., & Stevens, L. (1967) *J. Biol. Chem. 242*, 5460–5466.

Takenaka, T., Nogami, K., Gotoh, H., & Gotoh, R. (1971) *J. Colloid Interface Sci. 35*, 395–402.

Takenaka, T., Harada, K., & Matsumoto, M. (1980) *J. Colloid Interface Sci. 73*, 569–577.

Tamm, L. K. (1986) *Biochemistry 25*, 7470–7476.

Tsuboi, M. (1962) *J. Polymer Sci. 59*, 139.

Zbinden, R. (1964) *Infrared Spectroscopy of High Polymers*, Academic Press, New York.